Optimization of BGO Er/Yb doped pedestal waveguide amplifiers with Si nanostructures

1st Diego Silvério da Silva
Escola Politécnica
Universidade de São Paulo
São Paulo, Brazil
di.silverio@yahoo.com.br

2nd Luciana Reyes Pires Kassab
Departamento de Ensino Geral
Faculdade de Tecnologia de São Paulo
São Paulo, Brazil
kassablm@osite.com.br

3rd Ernesto Jimenez-Villar
Centro de Lasers e Aplicações
Instituto de Pesquisas Energéticas e Nucleares
São Paulo, Brazil
ernesto.jimenez@uv.es

4th Niklaus Ursus Wetter
Centro de Lasers e Aplicações
Instituto de Pesquisas Energéticas e Nucleares
São Paulo, Brazil
nuwetter@ipen.br

***Abstract*—In this work we review the recent advances in pedestal waveguide amplifier fabrication. The improvement of conventional photolithography and plasma etching methods brings advantages that benefit light guiding and reduce propagation losses, mainly in the 3rd telecommunication windows (λ~1550 nm). Yb^{3+}/Er^{3+} codoped Bi_2O_3-GeO_2 thin films, with and without Si nanostructures, are obtained by RF Magnetron sputtering deposition and are used as core layer of 500 nm height in the pedestal waveguides. Choosing an appropriate amount of these silicon nanostructures inside the rare-earth waveguides we achieve pump light scattering and at the same time very little scattering at the signal wavelength. The overall effect is again enhancement of 50% thus opening possibilities for potential applications in integrated optics.**

Keywords—Optical materials, Sputtering, Optical properties

I. INTRODUCTION

Doped fiber amplifiers such as Erbium Doped Fiber Amplifiers (EDFAs) and Ytterbium Doped Fiber Amplifiers (YDFAs) have been essential components of optical communication networks. In this way, Erbium doped waveguides amplifiers (EDWAs) have become extensively studied over the past years due to their promising applications in optical networks. New host materials based on heavy metals are of much interest in these areas [1] since they may present high nonlinear optical susceptibilities, which is important for applications like optical switching, wavelength conversion, parametric amplification among others [2-7].

There is a lack of studies concerning methodologies for EDWAs fabrication processes based on heavy metal oxide matrices. In this regard, pedestal waveguides are very promising, since their fabrication does not involve etching of the core layer [8].

For pedestal waveguides, reactive ion etching (RIE) occurs before the core definition, which represents an alternative method for achieving the lateral confinement in optical waveguides fabricated with silicon technology. The procedure represents an advantage when compared to rib waveguide production [9], since the material used as core layer does not need to be submitted to etching procedures, simplifying the fabrication process of the optical waveguides.

Recent studies based on pedestal waveguides fabricated with tellurite and germanate amorphous films also motivated the present work [1,8,10]. Another general lack of literature is related to research on heavy metal oxide glasses incorporating silicon nanostructures. This fact combined with progress in the photonics field in disordered optical media [11-13], lead us to a new strategy of photoluminescence (PL) and gain enhancement in Yb^{3+}/Er^{3+} codoped Bi_2O_3–GeO_2 (BGO) waveguides, which is provided through disorder and scattering caused by silicon nanostructures (NSs) formed in the sputtering process of the core.

Disorder in optical systems (elastic scattering) has given rise to new and interesting phenomena ranging from applications in solar collectors [14], random lasing [15,16], and other novel photonic functions, to investigations into fundamental topics, such as localization light [17-19]. Elastic scattering induces an increase in optical path length, which leads to an increase in the effective absorption and, in the stationary regime of population inversion gives also rise to an increase of gain [20,21]

II. MATERIALS AND METHODS

A. Pedestal waveguides fabrication process

The steps used for the pedestal waveguides fabrication process based on silicon technology are shown below [8,10].

1) Cleaning of the substrate surface

The cleaning of a P type silicon substrate with (100) orientation was realized to remove impurities like Na ions and metals (Fig 1.a).

2) Oxidation of the substrate surface

Thermal growth on a silicon substrate of a relatively thick silicon dioxide film (1~1.2 μm-thick) with refractive index of 1.46 was realized in order to obtain the cladding layer (Fig 1.b).

3) Cromium deposition

The Cr thin films were deposited using Magnetron RF Sputtering. This film serves as a mask and it is necessary since the photorresist is partially attacked during following the plasma corrosion process (Fig 1.c).

4) Photorresist deposition

Then the photoresist was deposited using a melt-spinner (Fig. 1d). After the solvent has evaporated, the photolithographic mask containing straight lines (with

978-1-7281-3092-7/19/$31.00©2019 IEEE

widths in the range of 1–100 µm) was aligned (Fig. 1e) with the wafer. The photoresist regions which were exposed to the UV light were sensitized during 10 s.

5) Removal of the photorresist

The developed solution AZ 351 (Microchemicals) was use to remove the sensitized photoresist (Fig 1f).

6) Removal of the chromium

The removal of exposed chromium was performed by wet etching process (Fig 1g).

7) Silicon dioxide corrosion

The pedestal structure was defined by the CHF3/O2 plasma etching using the Reactive Ion Etching (RIE) technique (Fig. 1h).

8) Removal of the remaining chromium

After the silicon oxide etching of the pedestal structures, the chromium film was removed using a ceric ammonium nitrate solution (Fig. 1i).

9) Core deposition

The last step consisted of Yb^{3+}/Er^{3+} codoped GeO_2–Bi_2O_3 deposition by RF Magnetron sputtering (Fig. 1j). This last procedure used the advances reported in references [1,8] that are: 1) reduction of the chromium mask thickness in 70% to reduce the micromasking effect and, 2) for the etching of the silicon dioxide an RF power of 100W and gas flow rate of 40 sccm for both CHF_3 and O_2, under a chamber pressure of 50 mTorr using 3 steps of 30 min instead of 2 steps.

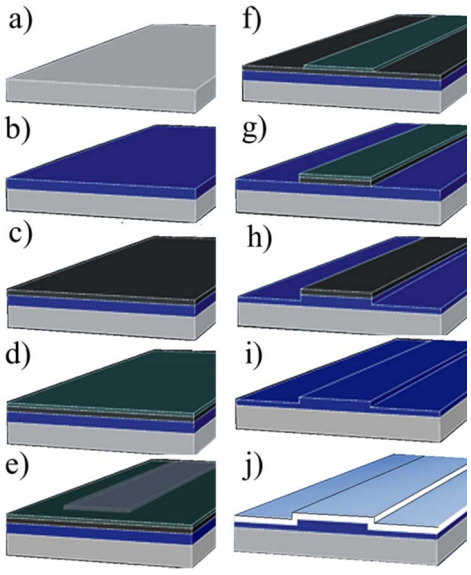

Fig. 1. Schematic diagram of the pedestal optical waveguide fabrication process: clean silicon substrate (a); cladding layer deposition (b); chromium film deposition (c); photoresist deposition (d); revelation of the photoresist (e); photoresist mask definition (f); chromium mask definition (g); etching of the SiO2 (h); chromium removal (i); core deposition (j).

B. *Microstructure characterization*

Scanning Electron Microscopy (SEM) was performed in order to observe the resulting structure of the pedestal-type waveguides. Figure 2 shows SEM images of the Er^{3+}/Yb^{3+} codoped BGO pedestal waveguide.

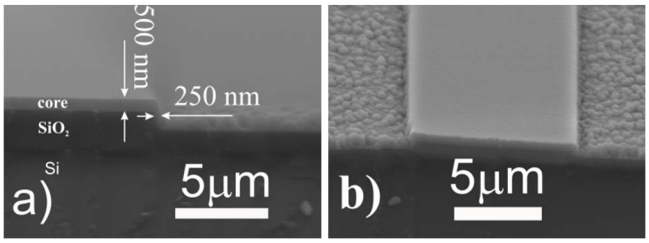

Fig. 2. SEM image of the Er^{3+}/Yb^{3+} codoped BGO pedestal waveguide. a) front view showing waveguide core dimensions. b) top view.

The higher refractive index of the waveguide containing Si should induce a decrease of the intrinsic losses of BGO waveguides at 1542 nm associated to the irregular morphology or defects at the waveguide borders. However, owing to the Si NSs that behave as a source of scattering, these may induce additional losses.

Additionally, the Si NSs should also provide inelastic scattering (absorption) at 980 nm (pumping), but at 1542 nm (gain) the absorption values should be small compared to shorter wavelengths as exemplified in figure 3.

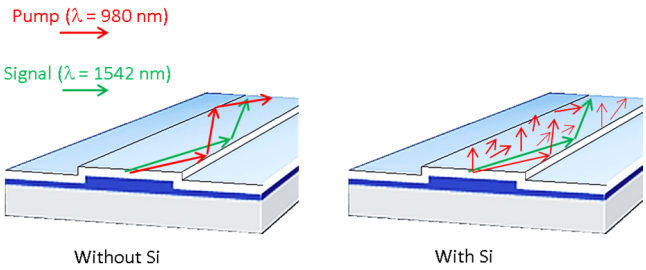

Fig. 3. Schematic view of the optical path-length increase in a waveguide with Si nanostructures (scatterers) in comparison with the one without Si nanostructures.

High resolution transmission electron microscopy (HR-TEM), electron diffraction pattern (EDP) analysis, energy dispersive spectroscopy (EDS) and small angle X ray scattering (SAXS) were performed in order to obtain information about the morphology and structure of the silicon NSs. Figure 4 shows HR-TEM images of the thin film waveguide containing Si nanostructures (500 nm thickness) where we observe Si aggregate with 25-35 nm size.

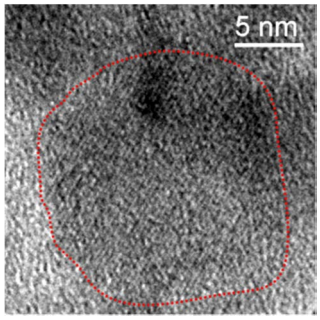

Fig. 4. HR-TEM images of the thin film waveguide containing Si nanostructures (500 nm thickness). Si aggregate with 25-35 nm size are observed. Dashed red lines were introduced for highlighting of the contours of Si aggregates.

III. RESULTS

The relative gain at 1542 nm was obtained using a 980 nm and 1542 nm for excitation and signal wavelengths, respectively with the experimental setup shown in figure 5.

The value of the relative gain is given by the ratio of the signal peak with and without 980 nm pumping [10]. Using the same setup the 980 nm pump absorption and the 1542 nm photoluminescence (PL) spectra were collected at very low pump powers from the top of the waveguide as a function of the longitudinal distance from the waveguide pump facet using a 200 µm diameter fiber, coupled to a spectrometer, in close proximity to the top surface.

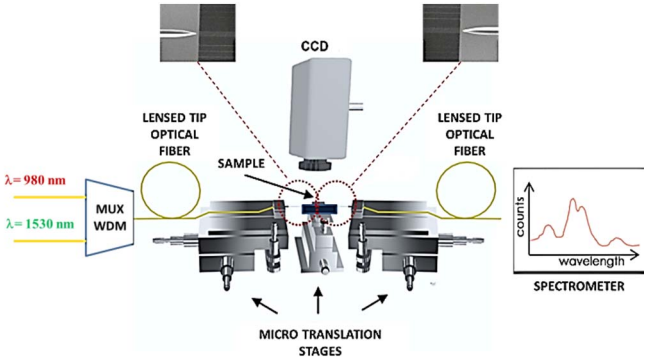

Fig. 5. Experimental setup used for gain and PL measurements

Figures 6a and 6b show PL results and relative gain of Er^{3+}/Yb^{3+} codoped BGO thin films with and without Si NSs, respectively. The large PL (Fig. 6a) increase at 1530 nm in the Si-nanostructures doped waveguide may be attributed to three main effects: i) increase of the effective optical path length due to the scattering provided by the Si NSs, leading to a absorption increase of Yb^{3+} ions; ii) decrease of $[Bi^{+}]$ and its respective absorption band (980 nm), increasing the effective pumping intensity for the Yb^{3+} ions inside the waveguide [12] and iii) smaller reabsorption at 1542 nm due to the decrease of $[Bi^{+}]$ and resulting decrease of $Er^{3+} \rightarrow Bi^{+}$ energy backtransfer [13,14]. The results presented in Fig. 6(b) show a higher slope for the waveguide with Si NSs, at lower pump powers and before the saturation. This result can be explained by the higher effective cross-section of the waveguide with Si NSs.

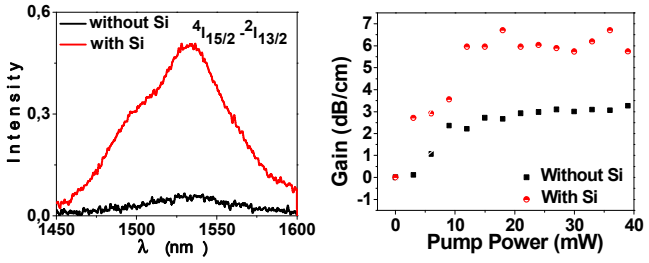

Fig. 6. Er^{3+}/Yb^{3+} codoped BGO thin films with and without Si (a) PL spectra, (b) Relative gain results at 1542 nm .

IV. CONCLUSION

This work investigated the fabrication and optical properties of Yb^{3+}/Er^{3+} codoped Bi_2O_3–GeO2 pedestal type waveguides for application with optical amplifiers. A method for producing Si NSs using the RF sputtering technique followed by an adequate heat treatment enabled the improvement of waveguide performance at 1542 nm of 50% obtaining a relative gain of 5.5 dB/cm. Large PL enhancement (~10 times) was observed in the visible and infrared regions.

The present work shows a strategy of increasing gain by introducing an appropriate amount of disorder caused by Si NSs and represents an alternative to the manufacture of more efficient amplifier waveguides and other advanced photonic devices.

Acknowledgements

We thank the financial support from FAPESP 2017/10765-5 and FAPESP 2013 26113-6; the Nanotechnology National Laboratory (LNNano) of the CNPEM-Campinas/Brazil, is also acknowledged for the HR-TEM measurements. We acknowledge INCT-Fotonica/CNPq.

REFERENCES

[1] F.A. Bomfim, D.M. da Silva, L.R.P. Kassab, T.A.A. de Assumpção, V.D. Del Cacho, M.I. Alayo, Advances on the fabrication process of Er3+/Yb3+:GeO2‑PbO pedestal waveguides for integrated photonics, Opt. Mater. 49 (2015) 196‑200.

[2] L.A. Florêncio, L.A. Gomez-Malagón, B.C. Lima, A.S.L. Gomes, J.A.M. Garcia, L.R.P. Kassab, Efficiency enhancement in solar cells using photon down-conversion in Tb/Yb-doped tellurite glass, Sol. Energy Mater. Sol. Cells 157 (2016) 468–475.

[3] H. Lin, S. Tanabe, L. Lin, Y.Y. Hou, K. Lin, D.L. Yang, T.C. Ma, J.Y. Yu, E.Y.B. Pun, Near-infrared emissions with widely different widths in two kinds of Er3+-doped oxide glasses with high refractive indices and low phonon energies, J. Lumin. 124 (2007) 167–172.

[4] M.E. Camilo, E.O. Silva, L.R.P. Kassab, J.A.M. Garcia, C.B. de Araújo, White light generation controlled by changing the concentration of silver nanoparticles hosted by Ho3+/Tm3+/Yb3+ doped GeO2–PbO glasses, J. Alloy. Compd. 644 (2015) 155–158.

[5] T.F. Xu, X. Shen, Q.H. Nie, Y. Gao, Spectral properties and thermal stability of Er^{3+}/Yb^{3+} codoped tungsten–tellurite glasses, Opt. Mater. 28 (2006) 241–245.

[6] L. Bontempo, S.G. dos Santos Filho, L.R.P. Kassab, Conduction and reversible memory phenomena in Au-nanoparticles-incorporated TeO_2–ZnO films, Thin Solid Films 611 (2016) 21–26.

[7] Y. Wu, X. Shen, S. Dai, Y. Xu, F. Chen, C. Lin, T.F. Xu, Q.H. Nie, Silver nanoparticles enhanced upconversion luminescence in Er3+/Yb3+ codoped bismuth-germanate glasses, J. Phys. Chem. 115 (2011) 25040–25045.

[8] M.E. Camilo, L.R.P. Kassab, T.A.A. Assumpção, V.D.D. Cacho, M.I. Alayo, Thin Solid Films 571 (2014) 225–229.

[9] D.M. da Silva, L.R.P. Kassab, A.L. Siarkowski, C.B. de Araújo, Influence of gold nanoparticles on the 1.53 µm optical gain in Er $^{3+}$/Yb $^{3+}$: PbO-GeO_2 RIB waveguides, Opt. Express 22 (2014) 16424–16430. doi:10.1364/OE.22.016424

[10] T.A.A. de Assumpção, M.E. Camilo, M.I. Alayo, D.M. da Silva, L.R.P. Kassab, Influence of gold nanoparticles on the 805 nm gain in Tm $^{3+}$/Yb^{3+} codoped PbO-GeO_2pedestal waveguides, Opt. Mater. (Amst). 72 (2017) 518–523. doi:10.1016/j.optmat.2017.06.031

[11] D.S. Wiersma, The physics and applications of random lasers, Nat. Phys. 4 (2008) 359–367. doi:10.1038/nphys971.

[12] E. Jimenez-Villar, I.F. Da Silva, V. Mestre, P.C. De Oliveira, W.M. Faustino, G.F. De Sa , Anderson localization of light in a colloidal suspension (TiO2@ silica), Nanoscale, vol. 8, pp. 10938-10946, 2016.

[13] N.U. Wetter, J.M. Giehl, F. Butzbach, D. Anacleto, E. Jimenez-Villar, Poly- dispersed powders (Nd 3þ :YVO 4) for ultra efficient random lasers, Part. Part. Syst. Char., vol. 4, pp. 1700335, 2017.

[14] H. Wang, et al., Single-crystalline rutile TiO2 hollow spheres: room-temperature synthesis, tailored visible-light- extinction, and effective scattering layer for quantum dot- sensitized solar cells, J. Am. Chem. Soc., vol. 133, pp. 19102-19109, 2011.

[15] E. Jimenez-Villar, I.F. Da Silva, V. Mestre, N.U. Wetter, C. Lopez, P.C. De Oliveira, W.M. Faustino, G.F. De S a, Random lasing at localization transition in a colloidal suspension (TiO2@Silica), ACS Omega, vol. 2, pp. 2415-2421, 2017.

[16] N.U. Wetter, A.R. de Miranda, E . Pecoraro, S.J.L. Ribeiro, E. Jimenez-Villar, Dynamic random lasing in silica aerogel doped with rhodamine 6G, RSC Adv., vol. 8, pp. 29678-29685, 2018.

[17] S. John, Electromagnetic absorption in a disordered medium near a photon mobility edge, Phys. Rev. Lett., vol. 53, pp. 2169-2172, 1984.

[18] E. Jimenez-Villar, M.C.S. Xavier, N.U. Wetter, V. Mestre, W.S. Martins, G.F. Basso, V.A. Ermakov, F.C. Marques, G.F. de Sa , Anomalous transport of light at the phase transition to localization: strong dependence with incident angle, Photon. Res., vol. 6, pp. 929-942, 2018.

[19] E. Jimenez Villar, M.C.S. Xavier, J.G.G.S. Ramos, N.U. Wetter, V. Mestre, W.S. Martins, G.F. Basso, V.A. Ermakov, F.C. Marques, G.F. de Sa , Localization of light: beginning of a new optics, in: D.L. Andrews, E.J. Galvez, J. Glückstad (Eds.), Complex Light Opt. Forces XII, Proceeding SPIE 10549, pp. 1054905, 2018.

[20] E. Jimenez-Villar, V. Mestre, P.C. de Oliveira, G.F. de S a, Novel core□shell (TiO2@Silica) nanoparticles for scattering medium in a random laser: higher efficiency, lower laser threshold and lower photodegradation, Nanoscale, vol. 5, pp. 12512-12517, 2013.

[21] E. Jimenez-Villar, V. Mestre, P.C. De Oliveira, W.M. Faustino, D.S. Silva, G.F. De S a, TiO2@Silica nanoparticles in a random laser: strong relationship of silica shell thickness on scattering medium properties and random laser performance, Appl. Phys. Lett., vol. 104, pp. 2-7, 2014.

[22] L.R.P. Kassab, M.E. Fukumoto, V.D.D. Cacho, N.U. Wetter, N.I. Morimoto,"Spectroscopic properties of Yb3+ doped PbO–Bi2O3–Ga2O3 glasses for IR laser applications," Opt. Mater., vol. 27, pp. 1576-1582, 2005.

[23] M. Peng, N. Zhang, L. Wondraczek, J. Qiu, Z. Yang, Q. Zhang, Ultrabroad NIR luminescence and energy transfer in Bi and Er/Bi co-doped germanate glasses, Opt. Express, vol. 19, pp. 20799, 2011.

[24] Emerson A. dos Santos, Lilia C. Courrol, Luciana R.P. Kassab, Laércio Gomes, Niklaus U. Wetter, Nilson D. Vieira, Sidney J.L. Ribeiro, Younes Messaddeq,"Evaluation of laser level populations of erbium-doped glasses," J. Lumin., vol. 124, pp. 200-206, 2007.